Hindawi
Advances in Polymer Technology
Volume 2019, Article ID 1316249, 14 pages
https://doi.org/10.1155/2019/1316249

Research Article

Investigations on Polymeric Nanoparticles for Ocular Delivery

Neeraj Mittal and Gurpreet Kaur

Department of Pharmaceutical Sciences and Drug Research, Punjabi University, Patiala 147002, Punjab, India

Correspondence should be addressed to Gurpreet Kaur; kaurgpt@gmail.com

Received 25 October 2018; Revised 10 April 2019; Accepted 5 May 2019; Published 2 June 2019

Academic Editor: Teresa Casimiro

In the present investigation, an attempt was made to formulate timolol maleate (TML) loaded polymeric nanoparticles of flax seed gum (FX) and chitosan (CH) for ocular delivery using ionic gelation method. The process of nanoparticle preparation was optimized using 2-factor, 3-level central composite experimental design. The optimal concentration of FX and CH that yielded nanoparticles with minimum particle size (267.06 ± 8.65 nm) and maximum encapsulation efficiency (74.96 ± 4.78%) was found to be 0.10% w/v and 0.08% w/v, respectively. The formulated nanoparticles revealed considerable bioadhesive strength and exhibited sustained release of drug in *in vitro* diffusion studies. The *ex vivo* transcorneal penetration study revealed higher corneal penetration of TML compared to marketed eye drops. The confocal scanning laser microscopy (CSLM) studies also confirmed the ability of nanoparticles to penetrate into deeper layers of cornea. The histopathological studies revealed corneal biocompatibility of nanoparticles. The nanoparticles were found to reduce the intra ocular pressure (IOP) in rabbits for prolonged period when compared to conventional eye drops. The results of the present study suggested a promising role of polymeric nanoparticles for ocular drug delivery in treatment of glaucoma.

1. Introduction

Polysaccharides are employed as promising excipients in pharmaceutical industries as gelling and suspending agents, emulsifier, binder, thickener, stabilizer, matrix former, and disintegrating agents [1]. The major advantage associated with the use of polysaccharides includes their abundant availability in nature, biodegradability, biocompatibility, and presence of groups that can be engineered for functionalization [2].

Flaxseed (*Linum usitatissimum* L.) gum (FX), a hydrocolloid extracted from flaxseed, is heterogeneous polysaccharide present in the outermost layer (epidermal layer) of flaxseed. The gum mainly comprises of xylose, arabinose, glucose, galactose, and rhamnose [3–5]. FX possesses number of advantages such as good water holding capacity, gelation, emulsifying, and foaming properties [6, 7]. Furthermore, it possesses a good nutrient value as dietary fiber and as a functional food ingredient. It has also been used to reduce risks associated with diabetes and heart disease [8, 9]. The functional properties of flaxseed gum are reported to be close to the gum arabic [10].

Chitosan (CH) is a natural, polycationic polymer widely employed in pharmaceutical formulations [11]. It is a deacetylated derivative of chitin, found abundantly in marine crustaceans, insects, and fungi [12, 13]. It is found to possess antibacterial, bioadhesive and permeability enhancing properties [14]. Researchers are working upon polyelectrolyte complexes of CH with other polysaccharides/polymers and their use as carriers for drug delivery. CH and carboxymethyl moringa gum polyelectrolyte complex based nanoparticles have been reported by Rimpy *et al.*, 2017, for the delivery of ofloxacin [15]. Similarly, pectin CH based nanoparticles have been observed to provide controlled release and improved antibacterial effectiveness of nisin [16].

Delivery of drugs to eye has been a challenging task due to complex anatomy and physiology of eye and presence of numerous barriers that limit the entry of drug molecule. Colloidal carriers like nanoparticles are gaining considerable attention lately, since they improve the patient compliance by avoiding ocular irritation, foreign body sensation, and reducing patient discomfort [17, 18]. However, these systems exhibit rapid clearance from eye leading to short residence time in

ocular mucosa [19]. The residence time of formulation can be enhanced by the use of bioadhesive polymers. Bioadhesive polymeric colloidal carriers have been reported to enhance the bioavailability of drug 1.71-fold as compared to colloidal carriers without bioadhesive polymers [20]. Studies carried out on CH based nanoparticles revealed excellent bioadhesive strength, sustained release of carteolol for 24 h resulting in prolonged reduction in intraocular pressure (IOP) as compared to drug solution in the treatment of glaucoma. Glaucoma is an emergent ocular disease, characterized by optic nerve damage. It is associated by an increase in IOP, which if left untreated can lead to loss of vision [21]. Timolol maleate (TML), a nonselective β-blocker, has been used for more than 30 years and still remains the drug of choice for glaucoma treatment. It lowers IOP by reducing the aqueous humour formation. However, TML has to be administered 4-6 times daily for prolonged therapeutic effect, since it is a short acting drug with elimination half-life of 2.5-5 h. [22]. The conventional ophthalmic eye drops are rapidly eliminated by blinking reflex, lacrimation, and drainage, which lead to short precorneal residence and poor bioavailability [23–25]. One of the approaches to improve therapeutic effectiveness of TML can be to increase the residence time of formulation employing bioadhesive polymers.

In this investigation, TML loaded bioadhesive polymeric nanoparticles were prepared by ionic gelation method using FX and CH for the treatment of glaucoma. The formulation was optimized using 2-factor 3-level central composite design. The optimized nanoparticles were further characterized by FTIR, DSC, SEM, TEM, XRD, and *in vitro* drug release studies. The reduction in IOP by polymeric nanoparticles was also determined employing suitable animal models.

2. Materials and Methods

2.1. Materials. Flax seeds were procured from local market. CH (MW 50,000-190,000 Da, degree of deacetylation ≥75%) and mucin were procured from Hi-Media Lab. Pvt. Ltd. (Mumbai, India). TML was received as a gift sample from Zee Laboratories Ltd., Poanta Sahib. Acetone and sodium bicarbonate were procured from Merck Specialties Pvt. Ltd., Mumbai. Calcium chloride dihydrate was purchased from LOBA Chemie Ltd., Mumbai.

2.2. Extraction and Purification of Flax Seed Gum (FX). Flax seed gum (FX) was extracted from the seeds of *Linum usitatissimum* by aqueous method. Flax seeds were first washed with water to remove any surface dust and then dried. The dried seeds were soaked in distilled water (8X) and stirred at 1000 rpm on magnetic stirrer for 3h at around 50°C. The viscous solution so formed was filtered employing muslin cloth. This was followed by centrifugation (4000 rpm) and precipitation of gum by addition of (50 ml × 2) acetone. The creamish/brownish colored precipitates so formed were separated by filtration, purified by dialysis, and dried in a lyophilizer (Allied Frost, Delhi) [26].

2.3. Characterization of FX and CH

2.3.1. Fourier Transform Infrared Spectroscopy (FTIR). FTIR spectrophotometer (NICOLET iS50, Thermo scientific) was employed to determine the spectral properties of powdered gum samples. A pellet of powdered samples mixed with KBr was compressed. The pellets were scanned over a frequency range of 4000–400 cm^{-1} [27].

2.3.2. Differential Scanning Calorimetry Analysis (DSC). The DSC of extracted gum and CH was recorded employing differential scanning calorimeter (EVO131, SETARAM Instrumentational France). Gum samples (2.0 mg) were heated from 20–400°C at a heating rate of 10°C/min under nitrogen purging rate of 10 ml/min [27].

2.3.3. X-Ray Diffraction (XRD). XRD was recorded on XPert PRO diffractometer system to analyze the crystallographic character of powdered gums. The experimental conditions employed included Cu Kα radiations (λ=1.54060 Å) generated at 45 kV and 40 mA, 2θ ranging from 5–50°, step size of 0.0170°, and scan step time of 24.7650 s at room temperature (25°C). The dried powdered samples were placed on sample stage (Spinner PW3064) and were evaluated for diffraction patterns [27].

2.3.4. Scanning Electron Microscopy (SEM). The morphological characteristics of the FX and CH were studied by scanning electron microscopy (JEOL, JSM- 6510LV). The samples were coated with gold (auto fine coater JFC-1600) to make it conductive. Images were captured at acceleration voltages of 5–10 kV electron beam [27].

2.3.5. Zeta Potential and pH Determination. The zeta potential of FX and CH (0.1% w/v) was measured using Zetasizer NanoZS90 (Malvern Instruments, UK). The gum samples were dispersed in HPLC water (Milli-Q Synergy Systems, Millipore) and the zeta potential measurements were performed by using an aqueous dip cell in an automatic mode. The temperature of the samples was controlled at 25°C. The pH of 1.0% (w/v) dispersion of FX and CH was measured using ESICO pH meter.

2.3.6. Interaction between FX and CH. A 1.0% w/v dispersion of FX and CH was prepared in water and acetic acid, respectively. The polymer dispersions (FX and CH) were mixed in the ratio of 10:90, 20:80, 30:70, 40:60, 50:50, 60:40, 70:30, 80:20, and 90:10 and allowed to stand. After 24 h, the supernatant was separated by centrifugation (Remi Cooling Centrifuge, India) at 10,000 rpm for 20 min. The precipitates were washed with distilled water and dried by lyophilization. The maximum ratio at which interaction took place was determined by measuring the viscosity of the supernatant using Brookfield viscometer (Spindle S18) and by calculating

Table 1: Various batches of polyelectrolyte complex nanoparticles with particle size and encapsulation efficiency.

S. No.	Factor 1 A:Concentration of FX (% w/v)	Factor 2 B:Concentration of CH (% w/v)	Response 1 Particle size (nm)	Response 2 Encapsulation efficiency (%)
1	0.12	0.05	270.8	79.33
2	0.08	0.05	170.5	58.22
3	0.16	0.02	485.2	83.27
4	0.16	0.08	412.5	89.72
5	0.08	0.08	209.8	63.19
6	0.12	0.05	311.4	72.29
7	0.12	0.08	298.5	88.36
8	0.12	0.05	208.3	81.88
9	0.16	0.05	502.7	91.13
10	0.12	0.05	281.9	76.03
11	0.08	0.02	180.3	51.11
12	0.12	0.02	212.6	53.55
13	0.12	0.05	309.6	82.16

the percentage yield of precipitates employing following equation [28, 29]:

$$percentage\ yield = \frac{\text{Wo}}{\text{Wt}} \times 100 \quad (1)$$

where W_0 = weight of precipitates obtained and Wt = total weight of polymers taken.

2.3.7. Formulation and Optimization of TML Loaded Nanoparticles. The polymeric nanoparticles of FX and CH were formulated employing ionic gelation method. FX and CH solutions were prepared by dissolving them into distilled water and acetic acid (2%, v/v), respectively. TML (0.5% w/v) was added to CH solution. Nanoparticles were prepared by adding FX solution (0.08-0.16% w/v) dropwise to the CH solution (0.02-0.08% w/v) under continuous stirring using a magnetic stirrer (800 rpm) at room temperature over a period of 30 min. The maximum interaction ratio of FX and CH (70:30) was used for the preparation of nanoparticles. Nanoparticles so formed were recovered by centrifugation at 11,000 rpm using ultracentrifuge for 40 min. The nanoparticles were then dried by lyophilization and stored until further use. Blank nanoparticles were also formulated using above method [30].

2.3.8. Design of Experiment (DoE). The optimization of polymeric nanoparticles was carried out using 2-factor, 3-level, central composite experimental design employing 13 runs (Table 1). Based upon preliminary screening (data not shown here), the concentration of FX (X1) and CH (X2) was chosen as the independent variables, and particle size (Y1) and encapsulation efficiency (Y2) were selected as dependent variables. The independent formulation variables were investigated at three levels (i.e., -1, 0, +1). The Design Expert Software (trial version 10.0) was used to optimize the experimental design and to analyze the data.

2.4. Characterization of Nanoparticles

2.4.1. Particle Size, Polydispersity Index, and Zeta Potential Analysis. The particle size, polydispersity index (PDI), and zeta potential of nanoparticles were determined employing Zetasizer (Malvern instruments, UK) using dynamic light scattering (DLS) technique at 25°C. Nanoparticles were dispersed in HPLC water and then analyzed.

2.4.2. Encapsulation Efficiency. For the measurement of encapsulation efficiency (EE), the suspension obtained after preparing nanoparticles was centrifuged at 11,000 rpm for 40 min at 4°C. The supernatant was analyzed for unentrapped drug spectrophotometrically at 294 nm [30]. The amount of encapsulated drug into the nanoparticles was calculated using following equation:

$$\text{EE} = \frac{\text{Total drug} - \text{Free drug}}{\text{Total drug added}} \times 100 \quad (2)$$

2.4.3. FTIR Analysis. The spectral properties of TML, blank nanoparticles, and drug loaded nanoparticles were analyzed employing a FTIR spectrophotometer (NICOLET iS50, Thermo scientific). The nanoparticles were mixed with KBr and a pellet was compressed. The pellets were scanned over a frequency range of 4000–400 cm^{-1} [27].

2.4.4. DSC. The thermal characteristics of TML, blank nanoparticles, and drug loaded nanoparticles were determined employing differential scanning calorimeter (EVO131, SETARAM Instrumentational France). The dried nanoparticles were crimped in a standard aluminium pan and heated from 20 to 400°C at 10°C/min under constant purging of nitrogen [27].

2.4.5. XRD. The crystallographic analysis of TML, blank nanoparticles, and optimized drug loaded nanoparticles

was carried out employing X-ray diffractogram (XPert PRO diffractometer) using similar conditions as mentioned above.

2.5. Morphological Studies. The surface morphology of the optimized formulation was observed using scanning electron microscopy (SEM) (JEOL, JSM-6510LV) and transmission electron microscopy (TEM) (HITACHI, H-7500). For SEM analysis, nanoparticles were taken and coated with gold (auto fine coater JFC-1600) to make them conductive. Images were taken at acceleration voltages of 5–10 kV electron beam. For TEM analysis, dispersion of nanoparticles was dropped on carbon coated copper grid and extra water was removed by blotting paper. Then grids containing the sample were scanned at 40-120 kV operating voltage and images were clicked at different resolution.

2.5.1. Measurement of Bioadhesive Strength. The bioadhesive strength was determined using texture analyzer equipped with a 50 kg load cell (TA.XT plus, Stable Micro Systems, UK). The cellophane membrane was mounted securely in place on a membrane tissue holder which was then wetted by mucin solution (0.3% w/v) (introduced by a micropipette). The pellets (1 cm^2) of FX-CH nanoparticles and FX and CH powders were compressed using single punch, hydraulic press through direct compression method, and then attached (using double sided adhesive tape) to the base of a cylindrical probe, which was fixed to the mobile arm of the texture analyzer. The cylindrical probe with the pellet attached to its base was lowered at a speed of 0.5 mm/s at a force of 1 N for a contact time of 2 min. It was then withdrawn at a rate of 0.5 mm/s to a distance of 10 mm. The mucoadhesive performance of the samples was determined by measuring the resistance to the withdrawal of the probe (maximum detachment force; F_{max} in Newton 'N') reflecting the mucoadhesion characteristics of the nanoparticles. At least three repetitions were obtained for each measurement.

2.6. In Vitro Diffusion Studies. In vitro diffusion studies were carried out using Keshary-Chein Franz diffusion cell. TML loaded nanoparticles (equivalent to 5 mg/ml of TML) dispersed in triple distilled water and marketed formulation (Iotim®) placed in donor compartment. Freshly prepared simulated tear fluid (sodium chloride 0.670 g, sodium bicarbonate 0.200 g, calcium chloride dihydrate 0.008 g, and purified water sufficient to make 100 mL) pH 7.2 was placed in receptor compartment of the Franz diffusion cell. The dialysis membrane was placed (0.22μm pore size) between the donor and receptor compartment. The temperature of the medium was maintained at 37°C ± 0.5°C. 2 ml of sample was withdrawn at predetermined time interval for 24 h and replaced with equal volume of fresh media. The withdrawn samples were analyzed after suitable dilution on UV spectrophotometer at 294 nm [31]. The amount of drug diffused was calculated using the equation generated ($y = 0.0131x + 0.0005$; $r^2 = 0.999$) from standard calibration curve and percentage release was determined.

2.7. Ex Vivo Transcorneal Permeation Studies. The freshly excised goat eyes were obtained from a local slaughter house. Cornea was removed carefully and washed several times with phosphate buffer (pH 7.4) to remove any proteinous matter. The excised cornea was mounted between the donor and receptor compartments of the Franz diffusion cell such that the endothelial surface of cornea faced the receptor compartment and epithelial towards the donor compartment. The optimized formulation (equivalent to 5 mg/ml of TML) and marketed formulation (Iotim®) were placed in donor compartment and freshly prepared simulated tear fluid pH 7.2 in receptor compartment. The temperature of the medium was maintained at 37°C ± 0.5°C. 2 ml of sample was withdrawn at predetermined time interval for 12 h from the cell and replaced with the equal volume of fresh media. The withdrawn samples were analyzed on UV spectrophotometer at 294 nm [31]. The amount of drug permeated was calculated using the equation generated from standard calibration curve and percentage drug permeated was determined.

2.8. Confocal Laser Scanning Microscopy (CLSM) Study. The corneal penetration of nanoparticles was determined using CLSM technique. Rhodamine 6G (0.03%) loaded nanoparticles (FX-CH-Rd) were prepared using same technique as above employing the optimized concentration of FX and CH. Goat cornea was placed between the donor and receptor compartments of the Franz diffusion cell. The dye loaded nanoparticles or a solution containing rhodamine 6G (Rd solution) was placed on the surface of the cornea in donor compartment as in the *ex vivo* transcorneal permeation study. The cornea was removed from diffusion assembly after 8 h and washed with phosphate buffer saline and immediately fixed with formalin solution (10% v/v). The tissue was dehydrated with alcohol, placed in melted paraffin, and solidified in block form. The cross sections of corneal tissue (<1 mm) were cut and fixed on the microscopic slide. The images were captured using confocal laser scanning microscope (Olympus FluoView FV 1000) with an argon laser beam of excitation at 480 nm and emission at 550 nm [32].

2.9. Corneal Toxicity Studies (Histopathology Study). Histopathology was done to check the irritation potential of nanoparticle formulation on goat cornea. The freshly excised goat eyes were obtained from a local slaughter house and kept in normal saline. The cornea was removed carefully and washed several times to remove any proteinous matter. The optimized formulation was incubated with excised cornea at 35°C for 1 h, followed by washing with phosphate buffer saline. The cornea was immediately fixed with formalin solution (10% v/v). The tissue was dehydrated with alcohol, placed in melted paraffin, and solidified in block form. The cross sections of corneal tissue (<1 mm) were cut, stained with hematoxylin and eosin. The cross sections of corneas incubated with phosphate buffer saline (negative control), sodium dodecyl sulfate, 0.1%, w/v (positive control), and marketed formulation (Iotim®) were prepared in the same manner. The corneal slides were evaluated under light microscope (Leica

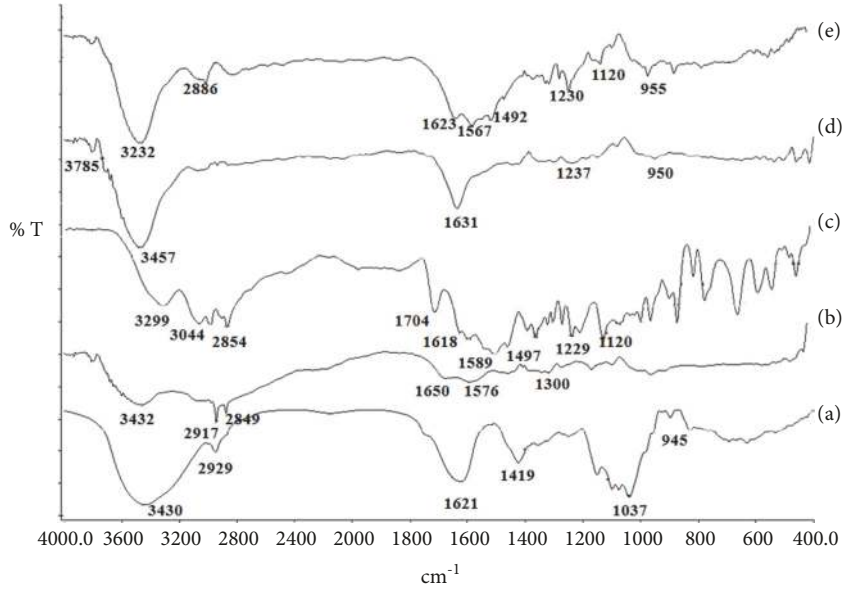

Figure 1: FTIR spectra of (a) FX, (b) CH, (c) TML, (d) blank nanoparticles, and (e) drug loaded optimized nanoparticles.

Microsystems CMS (DM 4000), Germany) and the images were captured [33].

2.10. In Vivo Studies. The protocol for *in vivo* studies was approved by Institutional animal ethical committee registration no. 107/99/CPCSEA-2012-30. Rabbits (1.5-2 kg) used for this study were housed under controlled conditions of temperature (20-25°C),and humidity and given free access to food and water. The reduction in IOP after administration of the optimized formulation and marketed formulation (Iotim®) of TML was determined employing HNT 7000 Non-Contact Tonometer. The study was carried out in normotensive albino rabbits [33]. Rabbits were divided into three groups each comprising three animals. The optimized formulation (50μl) was administered to the first group. The second group of animals received eye drops Iotim® (marketed formulation). The third group received blank nanoparticle formulation. The formulations were instilled on the corneal surface of one eye and contra lateral eye was kept as control. The change in IOP was recorded before the administration of drug loaded formulation and every hour after the instillation of drug formulation for a period of 12 h. All the measurements were recorded thrice and the mean values were taken. The percentage reduction in IOP was calculated by the following equation:

$$\text{Percentage decrease in IOP} = \frac{\text{IOP control eye} - \text{IOP treated eye}}{\text{IOP control eye}} \times 100 \quad (3)$$

2.11. Statistical Analysis. All the data are represented as mean ± standard deviation. Statistical analysis was done by employing ANOVA followed by Bonferroni (Posttest) test using Graph-pad PRISM software. A value of $p < 0.05$ or $p < 0.01$ was considered statistically significant.

3. Results and Discussion

3.1. Extraction of Flax Seed Gum (FX). The aqueous extraction technique used for the extraction of FX from the seeds of *Linum usitatissimum* L. resulted in a yield of 5.13 ± 0.15% w/w. The reported yield of FX from *Linum usitatissimum* L. varies from 3.6 to 8.0% w/w [34].

3.2. Characterization of FX. The FTIR spectra of FX (Figure 1(a)) showed sharp peaks at 3430 cm^{-1} and 2929 cm^{-1} which could be attributed to stretching of hydroxyl (-OH) groups of aliphatic alcohol and CH- groups of alkane, respectively. The peaks at 1621 cm^{-1} and 1419 cm^{-1} corresponding to C=O symmetric and asymmetric stretching, respectively, were also observed in spectra [35, 36]. All these peaks are in consonance with the peaks reported for arabic gum which has similar structure like FX [37]. The FTIR spectra of CH (Figure 1(b)) revealed a broad band of N-H stretching vibrations at 3432 cm^{-1}. The presence of C-H aliphatic stretching vibrations was observed at 2917 cm^{-1} and 2849 cm^{-1}. The characteristic bands of amide-I, amide-II, and amide-III were also evident at 1650 cm^{-1}, 1576 cm^{-1}, and 1300 cm^{-1}, respectively [38].

The DSC thermograms of FX (Figure 2(a)) and CH (Figure 2(b)) revealed a broad endotherm at 100.92°C and 102.19°C, respectively. An exothermic peak at 273.06°C and at 307.38°C was observed in thermogram of FX and CH, respectively. The endothermic peak could be associated to the loss of free/bound water present in the sample while the exothermic peak suggested the thermal degradation of the polymer.

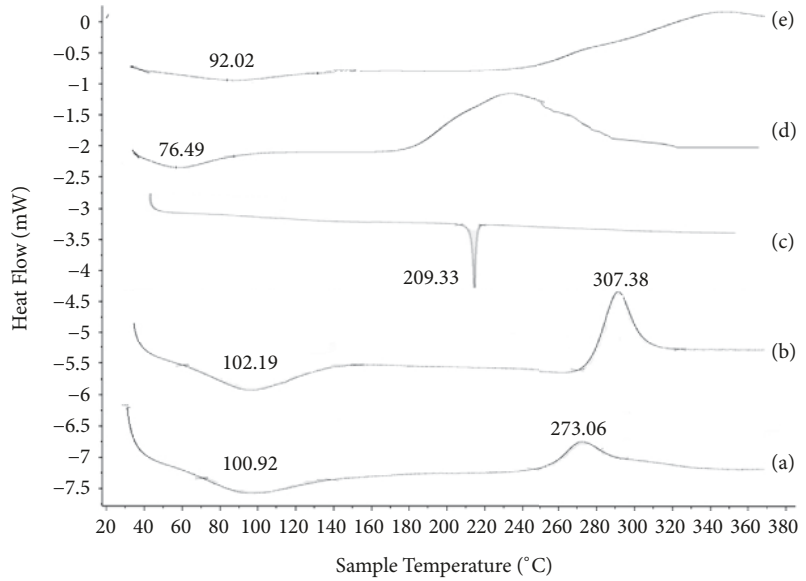

Figure 2: DSC of (a) FX, (b) CH, (c) TML, (d) blank nanoparticles, and (e) drug loaded optimized nanoparticles.

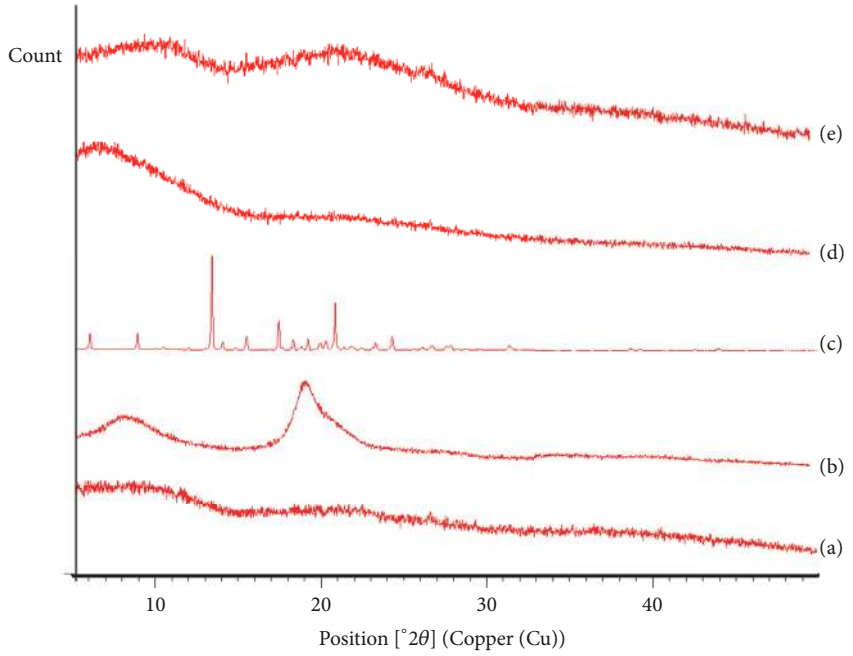

Figure 3: XRD of (a) FX, (b) CH, (c) TML, (d) blank nanoparticles, and (e) drug loaded optimized nanoparticles.

XRD is widely employed to determine the crystallinity and orientation of crystallites. The X-ray diffractogram of FX (Figure 3(a)) and CH (Figure 3(b)) revealed the amorphous nature of FX and crystalline nature of CH [39]. Natural polymers are reported to possess both amorphous and crystalline character, which was also confirmed from the SEM images of polymers (Figures 4(a) and 4(b)).

Zeta potential of the extracted gum was found to be -12.7 mV, which depicted its anionic nature while that of CH was found to be 12 mV. The pH of the FX and CH solution was found to be 6.78 ± 0.02 and 6.42 ± 0.04, respectively. The near neutral pH implies that it will not cause any irritation when used in the formulation.

3.3. Interaction Studies between FX and CH. The viscosity of the supernatants obtained after mixing solutions of FX with CH at different ratios is tabulated in Table 2. When oppositely charged polymers are mixed they undergo spontaneous reaction, resulting in the formation of precipitates [28]. The viscosity of the supernatant was observed to decrease as the proportion of FX in FX-CH mixture increased. At a ratio of 70:30 (FX:CH), the viscosity of the supernatant

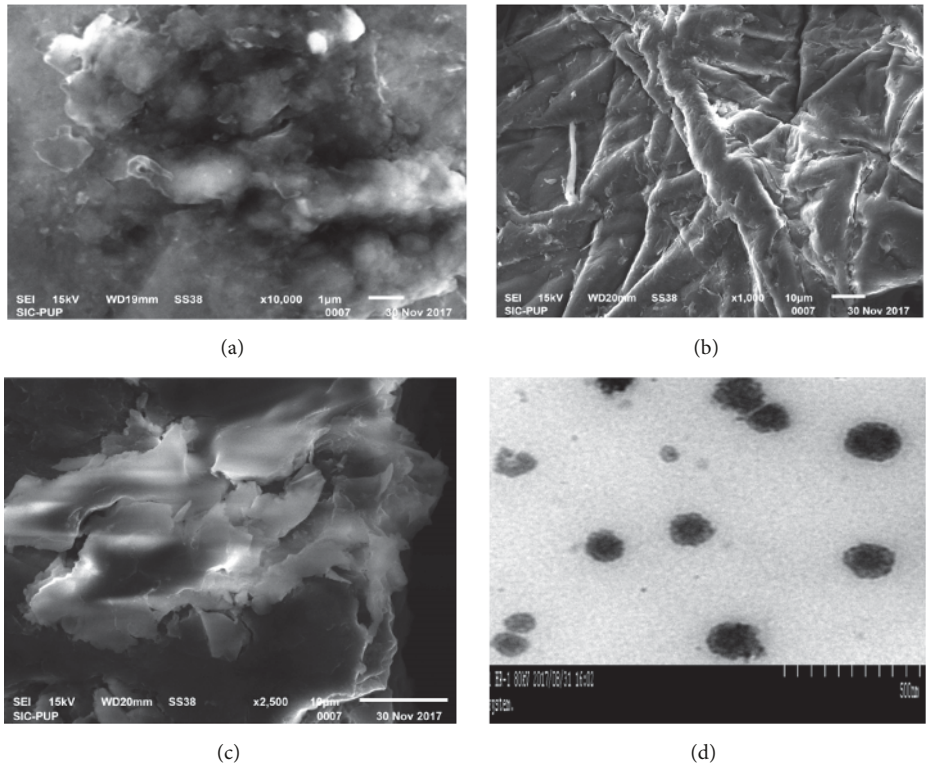

Figure 4: SEM images of (a) FX, (b) CH, and (c) drug loaded optimized nanoparticles and TEM image of (d) drug loaded optimized nanoparticles.

Table 2: Ratio of polymers with percentage yield and viscosity of FX-CH polyelectrolyte complexes.

S. No.	Ratio of Polymers (FX:CH)	Percentage (%) Yield	Viscosity (Cp)
1.	10:90	19.11 ± 2.03	9.22 ± 0.18
2.	20:80	41.07 ± 2.31	7.25 ± 0.13
3.	30:70	56.49 ± 2.73	4.39 ± 0.17
4.	40:60	72.64 ± 3.25	3.29 ± 0.13
5.	50:50	89.31 ± 1.84	2.43 ± 0.29
6.	60:40	94.56 ± 2.33	1.38 ± 0.06
7.	70:30	99.21 ± 1.46	1.17 ± 0.12
8.	80:20	77.24 ± 3.42	2.60 ± 0.24
9.	90:10	42.72 ± 2.41	5.75 ± 0.23

dropped to 1.17 ± 0.12 cP suggesting maximum interaction. The maximum percentage yield (99.21 ± 1.46%) was also observed at 70:30 ratio (FX:CH).

3.4. Preparation and Optimization of TML Loaded Nanoparticles. The nanoparticle formulations were prepared by a mild procedure of ionic gelation that involves an electrostatic interaction between oppositely charged polymers. This is a very simple procedure, involves mild preparation conditions, with complete hydrophilic environment, and avoids the use of organic solvents or high shear forces [40, 41].

Preliminary experiments were carried out to study the effect of variables (time, rpm, and concentration of polymers) on particle size and encapsulation efficiency (data not shown here). The results demonstrated that the concentration of FX and CH was significantly influencing the particle size and encapsulation efficiency of nanoparticles. The 2-factor, 3-level central composite experimental design was used to study the effect of concentration of FX (X1) and CH (X2) on particle size (Y1) and encapsulation efficiency (Y2). The results obtained after conducting 13 experimental runs as per the design protocol are summarized in Table 1. The results of dependent variables were fitted into various polynomial models, which emphasized that both the particle size (Y1) and encapsulation efficiency (Y2) fitted best into the linear model. The ANOVA analysis of the models revealed the model to be significant ($p < 0.05$) with nonsignificant 'lack of fit' ($p > 0.05$). The model reliability was confirmed by the higher

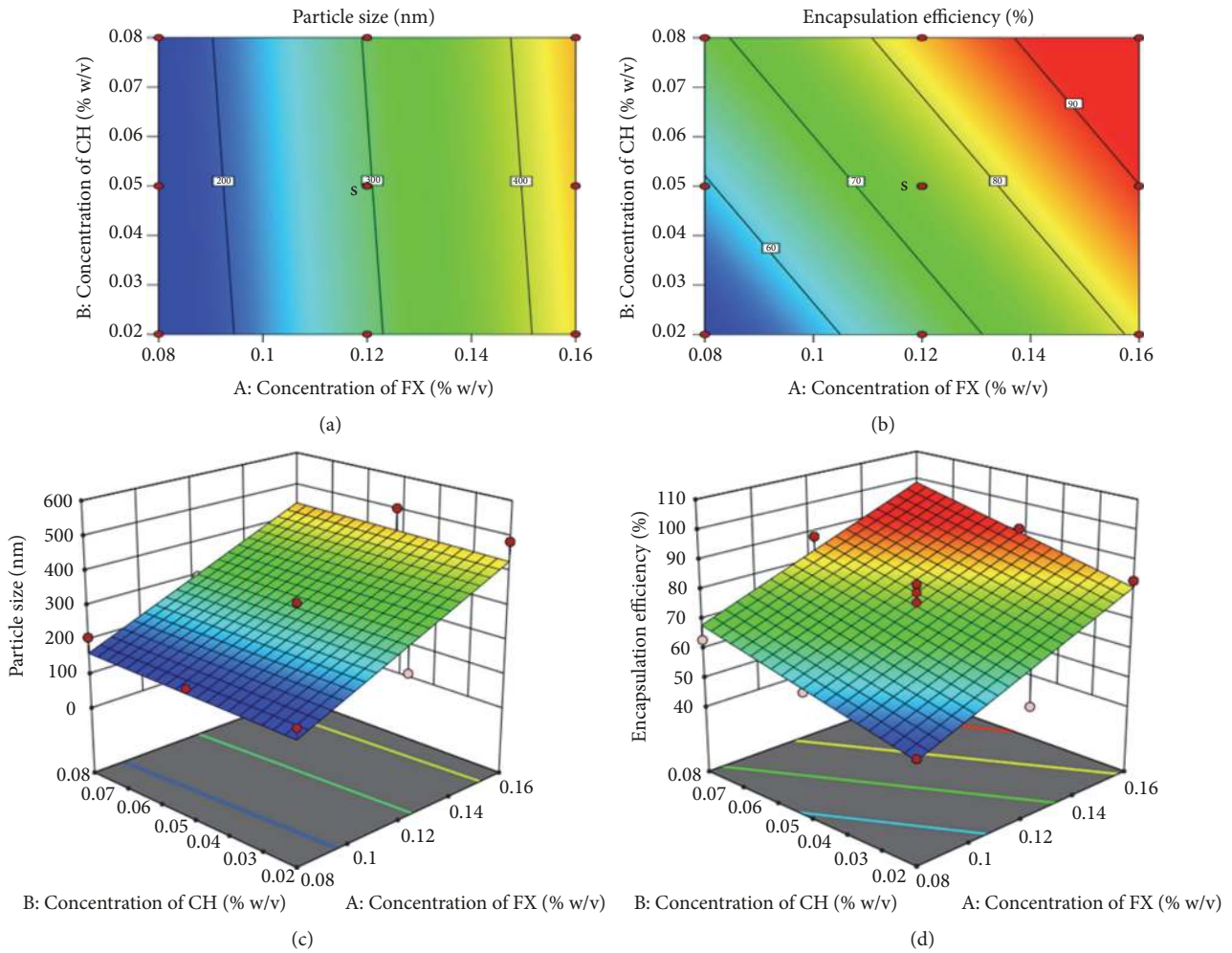

Figure 5: Response surface 2D and 3D contour graphs for particle size and encapsulation efficiency of FX-CH-TML nanoparticles.

values of R^2 and a reasonably good agreement between the adjusted R^2 and predicted R^2 values. In addition, the higher values of adequate precision (>4) showed adequate signal to noise ratio which suggested that the developed model can be used to navigate the design space.

3.5. Particle Size (Y1) and Encapsulation Efficiency (Y2). The mathematical relationship between the responses Y1 (Particle size), Y2 (Encapsulation efficiency), and independent variables X1 (concentration of FX) and X2 (concentration of CH) can be expressed by the following equations:

Particle size (Y1) = 296.47 + 139.97X1 + 7.12 X2

Encapsulation efficiency (Y2) = 74.63 + 15.27X1 + 8.89X2

Both the responses Y1 and Y2 were affected significantly by the change in X1 and X2. The response surface plots which showed a combined effect of concentration of FX and CH on particle size (Figures 5(a) and 5(c)) revealed that as the concentration of FX and CH increases the particle size also increases. The increase in particle size with increase in concentration of polymers could be attributed to the increase in viscosity of polymers and formation of aggregates. Furthermore, the availability of more binding sites for ionic cross linking of molecules could also be associated to increasing particle size [42]. An optimum level of concentration of FX and CH favour the formation of nanometric size particles. The combined effect of concentration of FX and CH on encapsulation efficiency (Figures 5(b) and 5(d)) of TML showed that with increase in concentration of polymers the encapsulation efficiency also increases. An increase in encapsulation efficiency with increasing concentration of polymers can also be explained similarly as above. The increasing viscosity of polymer solution with concentration prevents the leaching out of drug from the interacting gel phase into the bulk of the solution [43].

The optimal concentration of FX and CH to be employed for the preparation of nanoparticles with minimum particle size and maximum encapsulation efficiency was calculated using optimization tool of Design Expert Software. The design predicted the formulation with 0.10% (w/v) concentration of FX and 0.08% (w/v) concentration of CH to result in nanoparticles with a size of 254.5 nm and

encapsulation efficiency of 78.17%. Nanoparticle formulation (FX-CH-TML) employing the above concentration of FX and CH were prepared. The particle size of nanoparticles was found to be 267.06 ± 8.65 nm and encapsulation efficiency 74.96 ± 4.78%. The polydispersity index and zeta potential of this optimized batch were found to be 0.345 ± 0.02 and -20.3 ± 2.88 mV, respectively.

3.6. Characterization of Nanoparticles. FTIR spectra of TML (Figure 1(c)) showed a broad band at 3299 cm^{-1} corresponding to O-H/N-H stretching vibrations and the peaks at 2967 cm^{-1}, 2889 cm^{-1} and 2854cm^{-1} due to aliphatic C-H stretching vibrations. The band of carboxylic acid group of maleic acid was observed at 1704 cm^{-1} and C=N stretching vibrations were present at 1618 cm^{-1}. The bands at 1497 cm^{-1} and 1382 cm^{-1} were attributed to N–H bending vibrations and S-N group, respectively [44]. The strong peaks of TML at 1497 cm^{-1}, 1589 cm^{-1}, and 1618 cm^{-1} slightly shifted to 1492 cm^{-1}, 1567cm^{-1} and 1623 cm^{-1}, respectively, in drug loaded nanoparticles (Figure 1(e)) which clearly suggested that there is no ionic interaction between drug and polymers and the entrapment of drug is physical type [45, 46].

A sharp endotherm was shown by TML at 209.33°C (Figure 2(c)) which was not shown in optimized nanoparticles (Figure 2(e)). The disappearance of drug endotherm at 209.33°C in drug loaded nanoparticles could be attributed to the entrapment of drug into the polymer matrix [47]. This also indicated the amorphous dispersion of crystalline drug into the nanoparticles after encapsulation into the polymer [48].

XRD is widely employed to determine the percentage crystallinity and orientation of crystallites. The diffractogram of TML (Figure 3(c)) revealed its crystalline nature with sharp characteristic peaks. However, the crystallinity of TML was reduced in optimized nanoparticles (Figure 3(e)). The results are in consonance with DSC which suggested the encapsulation of drug within the nanoparticulate system [49].

The morphological studies (Figures 4(c) and 4(d)) revealed that nanoparticles were nanometric size (<100 nm) and possessed spherical and ovoid shape with no sharp edges, thus not expected to cause an irritation in cul-de-sac. The particle size observed under TEM (Figure 4(d)) was comparatively less as compared to DLS (267.06 ± 8.65 nm) since DLS measurements integrate the ionic environment surrounding the particle but in TEM analysis particle itself is focused [50, 51].

The bioadhesive properties of nanoparticles help in increasing the residence time of drug in cul-de-sac. It has been reported that, without bioadhesion, nanoparticles can be eliminated as quickly as aqueous solutions [52]. The bioadhesive strength of optimized nanoparticles, FX and CH, was found to be 713.91 ± 10.05 g, 272.77 ± 3.26 g, and 351.69 ± 4.43 g, respectively. The nanoparticles revealed considerable bioadhesive strength which could be attributed to increased flexibility of the polymeric chains and polar functional groups [53]. The nanoparticles exhibited negative zeta potential (-20.3 ± 2.88 mV) suggesting their anionic character. Earlier studies have concluded that the polyanions possess better bioadhesive strength as compared to polycations [54, 55]. Anionic polymers, e.g., poly (acrylic acid) and carboxymethyl cellulose, form strong hydrogen bonds with the mucin chains [56]. Furthermore, studies carried out by researchers suggest that uncoiling of the polymeric chains at near neutral pH in case of anionic polymers leads to greater bioadhesion through entanglement and penetration with the mucin [57].

3.7. In Vitro Diffusion Studies. The *in vitro* diffusion studies of the TML loaded optimized nanoparticle formulation (FX-CH-TML) showed an initial burst release (27.18% in 1 h) followed by sustained release (52.90% at 4 h, 67.71% at 8 h, 85.16% at 12 h and 90.55% at 24 h). The marketed formulation (Iotim®) released 49.35% in 1 h and 91.82% at the end of 4 h. The optimized nanoparticles were found to exhibit sustained release with statistically significant difference ($P<0.001$) in comparison to marketed formulation (Figure 6(a)). The initial burst release of drug from nanoparticles may be attributed to the presence of either drug particles on the surface of nanoparticles or weakly encapsulated within the polymeric matrix. The sustained release was observed due to hydration and swelling of polymers [58, 59]. The initial burst release of the drug is favourable for achieving the therapeutic concentration of TML in minimal time while the sustained release is required to maintain a minimal effective concentration for efficient glaucoma management [60].

3.8. Ex Vivo Studies. The *ex vivo* permeation studies were carried out using freshly excised goat cornea. The nanoparticle formulation (FX-CH-TML) showed 85.24% drug permeation through cornea within 12 h, on the other hand marketed formulation permeated 60.12% within 12 h (Figure 6(b)). The difference was statistically nonsignificant ($P>0.05$) till 0.5 h. However, a statistically significant ($P<0.001$) difference was observed after 0.5 h between the two formulations. The ability of the substance to permeate the corneal barrier depends on various factors like chemical nature of the substance, size, conformation, etc. It is reported that the submicron particles penetrate into the corneal epithelium cells by endocytosis [61]. The increased permeation from the nanoparticles as compared to solution (marketed formulation) may be because of higher retention of nanoparticles on the corneal surface due to nanosize of the particles and bioadhesion [62–64]. The presence of CH in formulation may also have contributed for increased penetration of drug due to its penetration enhancing property because of its ability to open the tight junctions located in epithelial cells [65].

3.9. CSLM Study. The corneal penetration of blank dye loaded nanoparticles and a solution containing rhodamine 6G was studied by CSLM study. The confocal images of cross sections of corneal tissue are depicted in Figure 7(I). The blank rhodamine loaded nanoparticles were found to penetrate to a greater extent into excised goat cornea (Figure 7(I)(a)) as compared to solution containing dye

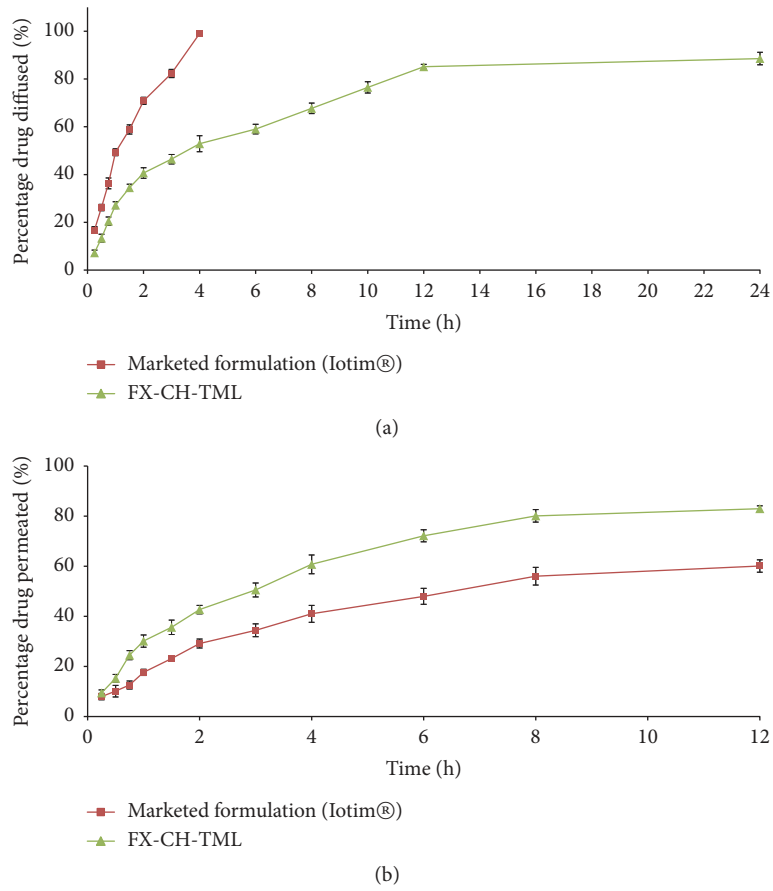

Figure 6: (a) *In vitro* drug release profile of TML from FX-CH-TML nanoparticles and marketed formulation; (b) *ex vivo* transcorneal permeation profile of TML from FX-CH-TML nanoparticles and marketed formulation.

(Figure 7(I)(b)). This could be attributed to small size of particles and penetration enhancing property of CH [66].

3.10. Histopathology Study. The cross sections of goat eye corneas treated with optimized formulation, marketed formulation, phosphate buffer saline (negative control), and sodium dodecyl sulfate (positive control) are shown in Figure 7(II). The corneal section incubated with sodium dodecyl sulfate showed a complete separation of superficial corneal epithelium (Figure 7(II)(d)). However, the optimized nanoparticles, marketed formulation, and phosphate buffer saline exhibited no change in the corneal cross sections. The corneal layers (epithelium, Bowman's membrane, and stroma) and cells were found to be intact and morphology of cornea was well maintained. The histopathological results advocate the safe use of polymeric nanoparticles for ocular drug delivery [67].

3.11. In Vivo Studies. The pharmacodynamic performance of optimized nanoparticles was determined by measuring reduction of intraocular pressure in rabbits employing HNT 7000 Non-Contact Tonometer. TML loaded nanoparticles and marketed formulation (Iotim® eye drops) were instilled only once to obtain relative comparison between single-dose administrations. The optimized nanoparticles and marketed formulation showed 18.79% and 19.99% IOP reduction after 1h, respectively. The maximum IOP (28.93%) reduction by optimized formulation (FX-CH-TML) was observed after 4 h whereas marketed formulation showed maximum IOP reduction (21.26%) after 3 h, however, the percentage IOP reduction was significantly lower as compared to optimized drug loaded nanoparticles. The results also suggested a significant difference ($P<0.001$) in IOP reduction after 3 h between both the formulations (Figure 8). A minimum 15% reduction in IOP is considered effective in glaucoma therapy [68]. Although the marketed formulation caused an immediate reduction in IOP, it was effective only for 4 h. The optimized nanoparticles, on the other hand, were effective for a period of 12 h. The improved effectiveness could be attributed to increased corneal contact time with bioadhesive polymeric nanoparticles.

4. Conclusion

Flax seed gum (FX) was isolated from *Linum usitatissimum* and characterized by FTIR, DSC, XRD, SEM, and zeta potential analysis. FX and CH nanoparticles were prepared

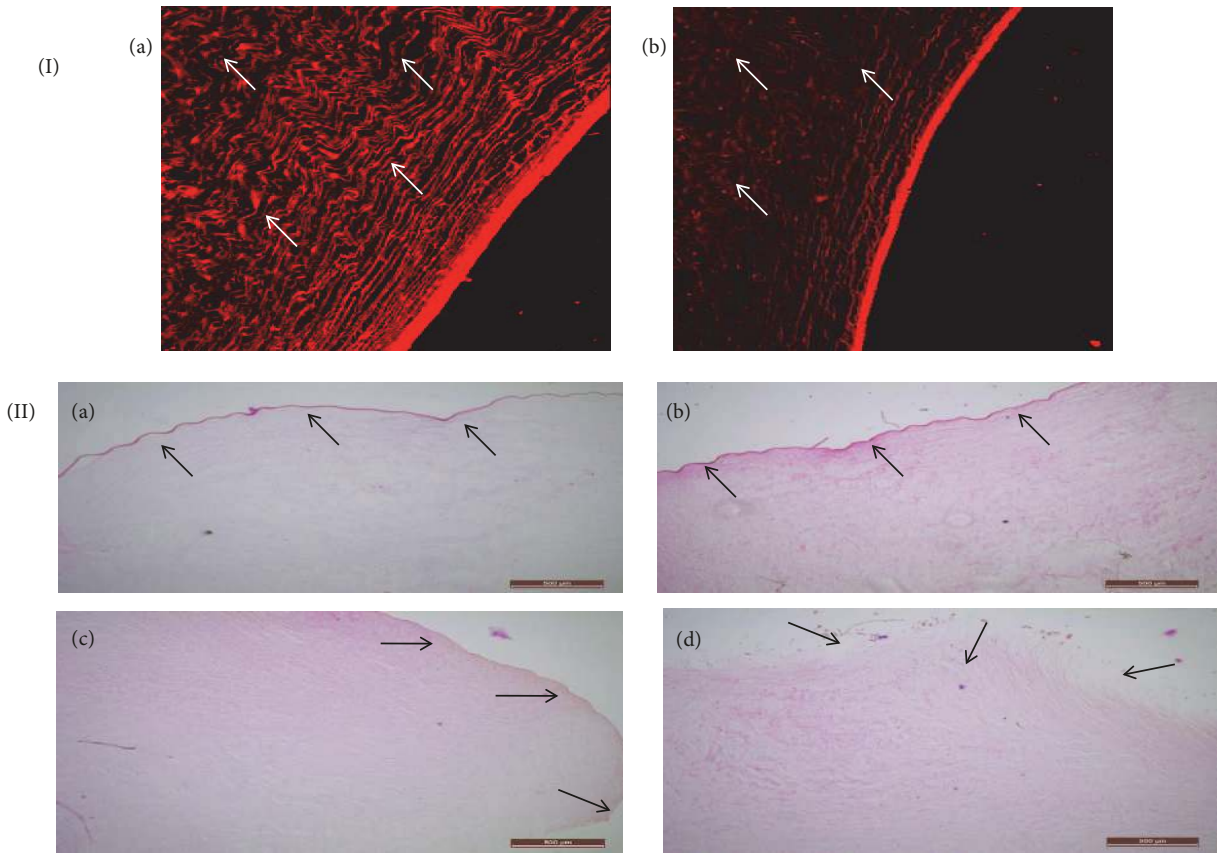

Figure 7: (I) CSLM image of rhodamine 6G loaded (a) FX-CH-Rd nanoparticles; (b) Rd solution; the arrows indicate the depth of penetration of rhodamine 6G; (II) cross section of cornea treated with (a) optimized formulation; (b) marketed formulation; (c) phosphate buffer saline (negative control); (d) sodium dodecyl sulfate (positive control); the arrows indicate the presence of intact corneal layers in (a), (b), and (c) and disrupted corneal layers in (d).

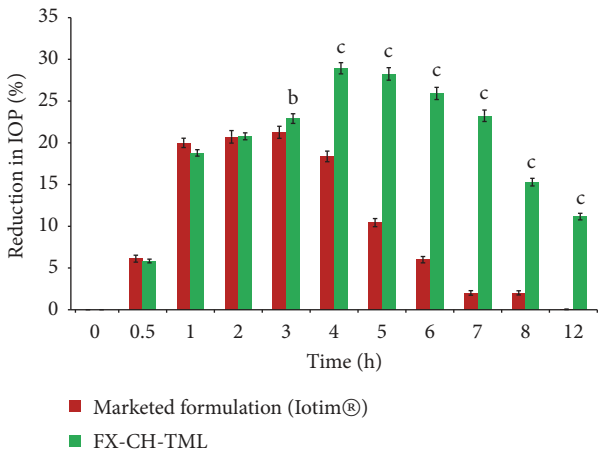

Figure 8: Percentage reduction in IOP (%) after administration of FX-CH-TML nanoparticles and marketed formulation (**b = $P < 0.01$; c = $P < 0.001$).

by ionic gelation method and the process was optimized using 2-factor, 3-level central composite experimental design. The optimized batch of nanoparticles was found to possess 267.06 ± 8.65 nm particle size and 74.96 ± 4.78% encapsulation efficiency. The bioadhesive polymeric nanoparticles exhibited appreciable bioadhesive property, sustained release of TML, and higher corneal penetration than marketed eye drops. The nanoparticles were biocompatible with cornea and showed greater and prolonged IOP reduction. The results of the present study suggested that the bioadhesive polymeric nanoparticles of FX and CH can be employed for ocular drug delivery in glaucoma treatment.

Data Availability

All the data used to support the findings of this study are included within the article.

Conflicts of Interest

The authors declare that they have no conflicts of interest.

Acknowledgments

The authors would like to acknowledge the Department of Science and Technology (DST, SERB), New Delhi (DST

No. SB/FT/LS-177/2012, Dated 26/04/2013), for providing the financial assistance.

References

[1] M. Yadav and M. Ahuja, "Preparation and evaluation of nanoparticles of gum cordia, an anionic polysaccharide for ophthalmic delivery," *Carbohydrate Polymers*, vol. 81, no. 4, pp. 871–877, 2010.

[2] T. R. Bhardwaj, M. Kanwar, R. Lal, and A. Gupta, "Natural gums and modified natural gums as sustained-release carriers," *Drug Development and Industrial Pharmacy*, vol. 26, no. 10, pp. 1025–1038, 2000.

[3] B. D. Oomah, E. O. Kenaschuk, W. Cui, and G. Mazza, "Variation in the composition of water-soluble polysaccharides in flaxseed," *Journal of Agricultural and Food Chemistry*, vol. 43, no. 6, pp. 1484–1488, 1995.

[4] A. J. Erskine and J. K. N. Jones, "The structure of linseed mucilage. Part I," *Canadian Journal of Chemistry*, vol. 35, no. 10, pp. 1174–1182, 1957.

[5] K. Hunt and J. K. N. Jones, "The structure of linseed mucilage: Part II," *Canadian Journal of Chemistry*, vol. 40, no. 7, pp. 1266–1279, 1962.

[6] J. Liu, Y. Y. Shim, T. J. Tse, Y. Wang, and M. J. T. Reaney, "Flaxseed gum a versatile natural hydrocolloid for food and non-food applications," *Trends in Food Science & Technology*, vol. 75, pp. 146–157, 2018.

[7] W. Cui, G. Mazza, and C. G. Biliaderis, "Chemical structure, molecular size distributions, and rheological properties of flaxseed gum," *Journal of Agricultural and Food Chemistry*, vol. 42, no. 9, pp. 1891–1895, 1994.

[8] B. D. Oomah, "Flaxseed as a functional food source," *Journal of the Science of Food and Agriculture*, vol. 81, no. 9, pp. 889–894, 2001.

[9] P. M. Stavro, A. L. Marchie, C. W. C. Kendall, V. Vuksan, and D. J. A. Jenkins, "Flaxseed, fiber and coronary heart disease: clinical studies," in *Flaxseed in Human Nutritio*, L. U. Thompson and S. C. Cunnane, Eds., pp. 288–300, AOCS Publishing, Illinois, IL, USA, 2nd edition, 2003.

[10] F. Bouaziz, M. Koubaa, F. J. Barba, S. Roohinejad, and S. E. Chaabouni, "Antioxidant properties of water-soluble gum from flaxseed hulls," *Antioxidants*, vol. 5, no. 3, p. 26, 2016.

[11] E. Başaran and Y. Yazan, "Ocular application of chitosan," *Expert Opinion on Drug Delivery*, vol. 9, no. 6, pp. 701–712, 2012.

[12] S. A. Agnihotri, N. N. Mallikarjuna, and T. M. Aminabhavi, "Recent advances on chitosan-based micro and nanoparticles in drug delivery," *Journal of Controlled Release*, vol. 100, no. 1, pp. 5–28, 2004.

[13] M. N. V. Ravi Kumar, "A review of chitin and chitosan applications," *Reactive & Functional Polymers*, vol. 46, no. 1, pp. 1–27, 2001.

[14] K. Reed, A. Li, B. Wilson, and T. Assamoi, "Enhancement of ocular in situ gelling properties of low acyl gellan gum by use of ion exchange," *Journal of Ocular Pharmacology and Therapeutics*, vol. 32, no. 9, pp. 574–582, 2016.

[15] Rimpy, Abhishek, and M. Ahuja, "Evaluation of carboxymethyl moringa gum as nanometric carrier," *Carbohydrate Polymers*, vol. 174, pp. 896–903, 2017.

[16] H. Wang, B. Yang, and H. Sun, "Pectin-Chitosan polyelectrolyte complex nanoparticles for encapsulation and controlled release of nisin," *American Journal of Polymer Science and Technology*, vol. 3, no. 5, pp. 82–88, 2017.

[17] R. Ilka, M. Mohseni, M. Kianirad, M. Naseripour, K. Ashtari, and B. Mehravi, "Nanogel-based natural polymers as smart carriers for the controlled delivery of Timolol Maleate through the cornea for glaucoma," *International Journal of Biological Macromolecules*, vol. 109, pp. 955–962, 2018.

[18] R. C. Nagarwal, S. Kant, P. N. Singh, P. Maiti, and J. K. Pandit, "Polymeric nanoparticulate system: a potential approach for ocular drug delivery," *Journal of Controlled Release*, vol. 136, no. 1, pp. 2–13, 2009.

[19] A. M. De Campos, A. Sánchez, and M. J. Alonso, "Chitosan nanoparticles: A new vehicle for the improvement of the delivery of drugs to the ocular surface. Application to cyclosporin A," *International Journal of Pharmaceutics*, vol. 224, no. 1-2, pp. 159–168, 2001.

[20] G. Tan, S. Yu, H. Pan et al., "Bioadhesive chitosan-loaded liposomes: a more efficient and higher permeable ocular delivery platform for timolol maleate," *International Journal of Biological Macromolecules*, vol. 94, pp. 355–363, 2017.

[21] Ameeduzzafar, J. Ali, A. Bhatnagar, N. Kumar, and A. Ali, "Chitosan nanoparticles amplify the ocular hypotensive effect of cateolol in rabbits," *International Journal of Biological Macromolecules*, vol. 65, pp. 479–491, 2014.

[22] M. Shokry, R. M. Hathout, and S. Mansour, "Exploring gelatin nanoparticles as novel nanocarriers for Timolol Maleate: augmented in-vivo efficacy and safe histological profile," *International Journal of Pharmaceutics*, vol. 545, no. 1-2, pp. 229–239, 2018.

[23] H. Almeida, M. H. Amaral, P. Lobão, and J. M. S. Lobo, "In situ gelling systems: a strategy to improve the bioavailability of ophthalmic pharmaceutical formulations," *Drug Discovery Therapy*, vol. 19, no. 4, pp. 400–412, 2014.

[24] Y. Wu, J. Yao, J. Zhou, and F. Z. Dahmani, "Enhanced and sustained topical ocular delivery of cyclosporine a in thermosensitive hyaluronic acid-based in situ forming microgels," *International Journal of Nanomedicine*, vol. 8, pp. 3587–3601, 2013.

[25] T. H. Tran, T. D. Nguyen, B. K. Poudel et al., "Development and evaluation of artesunate-loaded chitosan-coated lipid nanocapsule as a potential drug delivery system against breast cancer," *AAPS PharmSciTech*, vol. 16, no. 6, pp. 1307–1316, 2015.

[26] Y. Wang, D. Li, L.-J. Wang, M. Wu, and N. Özkan, "Rheological study and fractal analysis of flaxseed gum gels," *Carbohydrate Polymers*, vol. 86, no. 2, pp. 594–599, 2011.

[27] N. Mittal, P. Mattu, and G. Kaur, "Extraction and derivatization of Leucaena leucocephala (Lam.) galactomannan: optimization and characterization," *International Journal of Biological Macromolecules*, vol. 92, pp. 831–841, 2016.

[28] G. Kaur, S. Jain, and A. K. Tiwary, "Chitosan-carboxymethyl tamarind kernel powder interpolymer complexation: Investigations for colon drug delivery," *Scientia Pharmaceutica*, vol. 78, no. 1, pp. 57–78, 2010.

[29] K. Kaur and G. Kaur, "Formulation and evaluation of chitosan-chondroitin sulphate based nasal inserts for zolmitriptan," *BioMed Research International*, vol. 2013, Article ID 958465, 2013.

[30] S. K. Motwani, S. Chopra, S. Talegaonkar, K. Kohli, F. J. Ahmad, and R. K. Khar, "Chitosan-sodium alginate nanoparticles as submicroscopic reservoirs for ocular delivery: formulation, optimisation and in vitro characterisation," *European Journal of*

Pharmaceutics and Biopharmaceutics, vol. 68, no. 3, pp. 513–525, 2008.

[31] S. Katiyar, J. Pandit, R. S. Mondal et al., "In situ gelling dorzolamide loaded chitosan nanoparticles for the treatment of glaucoma," *Carbohydrate Polymers*, vol. 102, no. 1, pp. 117–124, 2014.

[32] A. Ahad, M. Aqil, K. Kohli, Y. Sultana, M. Mujeeb, and A. Ali, "Formulation and optimization of nanotransfersomes using experimental design technique for accentuated transdermal delivery of valsartan," *Nanomedicine: Nanotechnology, Biology and Medicine*, vol. 8, no. 2, pp. 237–249, 2012.

[33] M. H. Warsi, M. Anwar, V. Garg et al., "Dorzolamide-loaded PLGA/vitamin E TPGS nanoparticles for glaucoma therapy: Pharmacoscintigraphy study and evaluation of extended ocular hypotensive effect in rabbits," *Colloids and Surfaces B: Biointerfaces*, vol. 122, pp. 423–431, 2014.

[34] K.-Y. Qian, S. W. Cui, J. Nikiforuk, and H. D. Goff, "Structural elucidation of rhamnogalacturonans from flaxseed hulls," *Carbohydrate Research*, vol. 362, pp. 47–55, 2012.

[35] M. Kačuráková, P. S. Belton, R. H. Wilson, J. Hirsch, and A. Ebringerová, "Hydration properties of xylan-type structures: an FTIR study of xylooligosaccharides," *Journal of the Science of Food and Agriculture*, vol. 77, no. 1, pp. 38–44, 1998.

[36] D. Mudgil, S. Barak, and B. S. Khatkar, "X-ray diffraction, IR spectroscopy and thermal characterization of partially hydrolyzed guar gum," *International Journal of Biological Macromolecules*, vol. 50, no. 4, pp. 1035–1039, 2012.

[37] C. A. Ibekwe, G. M. Oyatogun, T. A. Esan, and K. M. Oluwasegun, "Synthesis and characterization of chitosan/gum arabic nanoparticles for bone regeneration," *American Journal of Materials Science and Engineering*, vol. 5, no. 1, pp. 28–36, 2017.

[38] S. Jana, A. Banerjee, and A. Gandhi, "Preparation and characterization of chitosan based polyelectrolyte complex as a carrier of acetoclofenac," *Journal of PharmaSciTech*, vol. 3, no. 2, p. 68, 2014.

[39] B. Hastuti and D. Siswanta, "Synthesis and characterization pectin-carboxymethyl chitosan crosslinked pegde as biosorbent of Pb(II) ion," *IOP Conference Series: Materials Science and Engineerin*, vol. 299, no. 1, p. 012052, 2018 (Arabic).

[40] A. Grenha, "Chitosan nanoparticles: A survey of preparation methods," *Journal of Drug Targeting*, vol. 20, no. 4, pp. 291–300, 2012.

[41] C. Prego, D. Torres, and M. J. Alonso, "The potential of chitosan for the oral administration of peptides," *Expert Opinion on Drug Delivery*, vol. 2, no. 5, pp. 843–854, 2005.

[42] A. R. Dudhani and S. L. Kosaraju, "Bioadhesive chitosan nanoparticles: Preparation and characterization," *Carbohydrate Polymers*, vol. 81, no. 2, pp. 243–251, 2010.

[43] Minkal, M. Ahuja, and D. C. Bhatt, "Carboxymethyl gum katira: synthesis, characterization and evaluation for nanoparticulate drug delivery," *RSC Advances*, vol. 5, no. 100, pp. 82363–82373, 2015.

[44] P. Mehta, A. A. Al-Kinani, R. Haj-Ahmad et al., "Electrically atomised formulations of timolol maleate for direct and on-demand ocular lens coatings," *European Journal of Pharmaceutics and Biopharmaceutics*, vol. 119, pp. 170–184, 2017.

[45] U. Shinde, M. H. Ahmed, and K. Singh, "Development of dorzolamide loaded 6-O-carboxymethyl chitosan nanoparticles for open angle glaucoma," *Journal of Drug Delivery*, vol. 2013, Article ID 562727, 15 pages, 2013.

[46] P. Zhang, X. Liu, W. Hu, Y. Bai, and L. Zhang, "Preparation and evaluation of naringenin-loaded sulfobutylether-β-cyclodextrin/chitosan nanoparticles for ocular drug delivery," *Carbohydrate Polymers*, vol. 149, pp. 224–230, 2016.

[47] H. Gupta, M. Aqil, R. K. Khar, A. Ali, A. Bhatnagar, and G. Mittal, "Sparfloxacin-loaded PLGA nanoparticles for sustained ocular drug delivery," *Nanomedicine: Nanotechnology, Biology and Medicine*, vol. 6, no. 2, pp. 324–333, 2010.

[48] R. Zhao, J. Li, J. Wang, Z. Yin, Y. Zhu, and W. Liu, "Development of timolol-loaded galactosylated chitosan nanoparticles and evaluation of their potential for ocular drug delivery," *AAPS PharmSciTech*, vol. 18, no. 4, pp. 997–1008, 2017.

[49] A. K. Sah, P. K. Suresh, and V. K. Verma, "PLGA nanoparticles for ocular delivery of loteprednol etabonate: a corneal penetration study," *Artificial Cells, Nanomedicine and Biotechnology*, vol. 45, no. 6, pp. 1156–1164, 2017.

[50] A. Gèze, J.-L. Putaux, L. Choisnard, P. Jéhan, and D. Wouessidjewe, "Long-term shelf stability of amphiphilic β-cyclodextrin nanosphere suspensions monitored by dynamic light scattering and cryo-transmission electron microscopy," *Journal of Microencapsulation*, vol. 21, no. 6, pp. 607–613, 2004.

[51] N. Dilbaghi, H. Kaur, M. Ahuja, and S. Kumar, "Evaluation of tropicamide-loaded tamarind seed xyloglucan nanoaggregates for ophthalmic delivery," *Carbohydrate Polymers*, vol. 94, no. 1, pp. 286–291, 2013.

[52] A. Patel, K. Cholkar, V. Agrahari, and A. K. Mitra, "Ocular drug delivery systems: an overview," *World Journal of Pharmacology*, vol. 2, no. 2, pp. 47–64, 2013.

[53] S. Wittaya-Areekul, J. Kruenate, and C. Prahsarn, "Preparation and in vitro evaluation of mucoadhesive properties of alginate/chitosan microparticles containing prednisolone," *International Journal of Pharmaceutics*, vol. 312, no. 1-2, pp. 113–118, 2006.

[54] N. A. Peppas and P. A. Buri, "Surface, interfacial and molecular aspects of polymer bioadhesion on soft tissues," *Journal of Controlled Release*, vol. 2, pp. 257–275, 1985.

[55] S. H. S. Leung and J. R. Robinson, "The contribution of anionic polymer structural features to mucoadhesion," *Journal of Controlled Release*, vol. 5, no. 3, pp. 223–231, 1987.

[56] S. Mansuri, P. Kesharwani, K. Jain, R. K. Tekade, and N. K. Jain, "Mucoadhesion: A promising approach in drug delivery system," *Reactive and Functional Polymers*, vol. 100, pp. 151–172, 2016.

[57] K. M. Tur and H.-S. Ch'ng, "Evaluation of possible mechanism(s) of bioadhesion," *International Journal of Pharmaceutics*, vol. 160, no. 1, pp. 61–74, 1998.

[58] G. Abrego, H. L. Alvarado, M. A. Egea, E. Gonzalez-Mira, A. C. Calpena, and M. L. Garcia, "Design of nanosuspensions and freeze-dried PLGA nanoparticles as a novel approach for ophthalmic delivery of pranoprofen," *Journal of Pharmaceutical Sciences*, vol. 103, no. 10, pp. 3153–3164, 2014.

[59] M. Amidi, S. G. Romeijn, G. Borchard, H. E. Junginger, W. E. Hennink, and W. Jiskoot, "Preparation and characterization of protein-loaded N-trimethyl chitosan nanoparticles as nasal delivery system," *Journal of Controlled Release*, vol. 111, no. 1-2, pp. 107–116, 2006.

[60] S. Shi, Z. Zhang, Z. Luo et al., "Chitosan grafted methoxy poly(ethylene glycol)-poly(ε-caprolactone) nanosuspension for ocular delivery of hydrophobic diclofenac," *Scientific Reports*, vol. 5, p. 11337, 2015.

[61] P. Calvo, M. J. Alonso, J. L. Vila-Jato, and J. R. Robinson, "Improved ocular bioavailability of indomethacin by novel

ocular drug carriers," *Journal of Pharmacy and Pharmacology*, vol. 48, no. 11, pp. 1147–1152, 1996.

[62] J. V. Aukunuru and U. B. Kompella, "In vitro delivery of nano- and micro-particles to retinal pigment epithelial (RPE) cells," *Drug Delivery and Technology*, vol. 2, no. 2, pp. 50–57, 2002.

[63] M. G. Qaddoumi, H. J. Gukasyan, J. Davda, V. Labhasetwar, K.-J. Kim, and V. H. L. Lee, "Clathrin and caveolin-1 expression in primary pigmented rabbit conjunctival epithelial cells: Role in PLGA nanoparticle endocytosis," *Molecular Vision*, vol. 9, pp. 559–568, 2003.

[64] F. Rafie, Y. Javadzadeh, A. R. Javadzadeh et al., "In vivo evaluation of novel nanoparticles containing dexamethasone for ocular drug delivery on rabbit eye," *Current Eye Research*, vol. 35, no. 12, pp. 1081–1089, 2010.

[65] M. de la Fuente, M. Raviña, P. Paolicelli, A. Sanchez, B. Seijo, and M. J. Alonso, "Chitosan-based nanostructures: A delivery platform for ocular therapeutics," *Advanced Drug Delivery Reviews*, vol. 62, no. 1, pp. 100–117, 2010.

[66] G. K. Jain, S. A. Pathan, S. Akhter et al., "Microscopic and spectroscopic evaluation of novel PLGA-chitosan Nanoplexes as an ocular delivery system," *Colloids and Surfaces B: Biointerfaces*, vol. 82, no. 2, pp. 397–403, 2011.

[67] Ameeduzzafar, S. S. Imam, S. N. Abbas Bukhari, J. Ahmad, and A. Ali, "Formulation and optimization of levofloxacin loaded chitosan nanoparticle for ocular delivery: in-vitro characterization, ocular tolerance and antibacterial activity," *International Journal of Biological Macromolecules*, vol. 108, pp. 650–659, 2018.

[68] A. Akman, A. Cetinkaya, Y. A. Akova, and A. Ertan, "Comparison of additional intraocular pressure-lowering effects of latanoprost vs brimonidine in primary open-angle glaucoma patients with intraocular pressure uncontrolled by timolol-dorzolamide combination," *Eye*, vol. 19, no. 2, pp. 145–151, 2005.